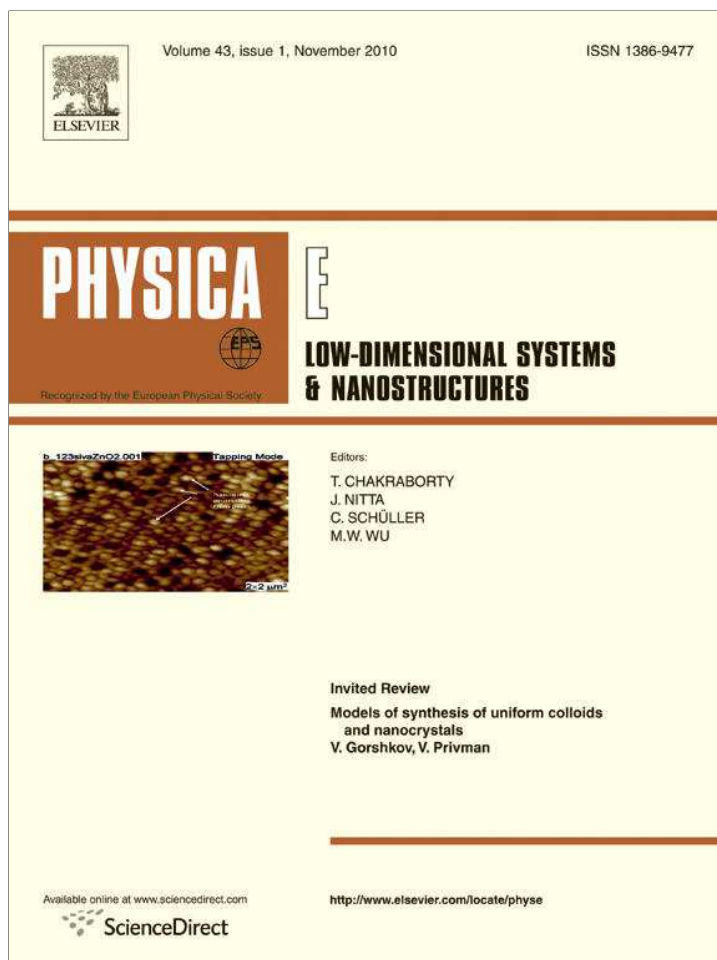


Provided for non-commercial research and education use.
Not for reproduction, distribution or commercial use.



This article appeared in a journal published by Elsevier. The attached copy is furnished to the author for internal non-commercial research and education use, including for instruction at the authors institution and sharing with colleagues.

Other uses, including reproduction and distribution, or selling or licensing copies, or posting to personal, institutional or third party websites are prohibited.

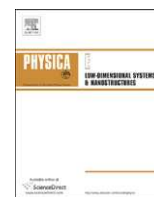
In most cases authors are permitted to post their version of the article (e.g. in Word or Tex form) to their personal website or institutional repository. Authors requiring further information regarding Elsevier's archiving and manuscript policies are encouraged to visit:

<http://www.elsevier.com/copyright>



Contents lists available at ScienceDirect

Physica E

journal homepage: www.elsevier.com/locate/phys

Titania nanotubes modeled from 3- and 6-layered (1 0 1) anatase sheets: Line group symmetry and comparative *ab initio* LCAO calculations

R.A. Evarestov^{a,*}, A.V. Bandura^a, M.V. Losev^a, S. Piskunov^{b,c,d}, Yu.F. Zhukovskii^b

^a Department of Quantum Chemistry, St. Petersburg State University, 26 Universitetsky Prospect, Petrodvorets 198504, Russia

^b Institute of Solid State Physics, University of Latvia, 8 Kengaraga Street, Riga LV-1063, Latvia

^c Faculty of Computing, University of Latvia, 19 Raina Blvd., Riga LV-1586, Latvia

^d Faculty of Physics and Mathematics, University of Latvia, 8 Zellu Str., Riga LV-1002, Latvia

ARTICLE INFO

Article history:

Received 22 December 2009

Received in revised form

16 July 2010

Accepted 29 July 2010

Available online 4 August 2010

ABSTRACT

The formalism of line groups for one-periodic (1D) nanostructures with rotohelical symmetry has been applied for construction of TiO₂ nanotubes (NTs). They are formed by rolling up the stoichiometric two-periodic (2D) sheets cut from the energetically stable (1 0 1) anatase surface, which contains either six (O–Ti–O–O–Ti–O) or three (O–Ti–O) layers. After optimization of geometry the former keeps the centered rectangular symmetry of initial slab while the latter is spontaneously reconstructed to the hexagonal fluorite-type (1 1 1) sheet. We have considered the four sets of TiO₂ NTs with optimized 6- and 3-layered structures, which possess the two pairs of either anatase (–*n*,*n*) and (*n*,*n*) or fluorite (*n*,*n*) and (*n*,0) chiralities, respectively. To analyze their structural and electronic properties, we have performed *ab initio* LCAO calculations on titania slabs and nanotubes using the hybrid Hartree-Fock/Kohn-Sham exchange-correlation functional PBE0. Both band gaps and strain energies of these nanotubes have been computed as functions of NT diameter consequently changed from 0.5 nm to 4.0 nm with number of atoms *per* nanotube unit cell increased from 30 up to 288. A ratio of the calculated strain energies between the 3- and 6-layered titania NTs achieves 2–3 for nanotubes with diameters ≤ 1.0 nm and remains noticeable for those with diameters ≤ 2.0 nm, *i.e.*, the latter are more stable energetically. When diameters of nanotubes increase up to 4.0 nm these strain energies substantially decrease and approach each other. At the same time, the strain energy of 6-layered NTs with (–*n*,*n*) chirality is smaller than that for (*n*,*n*) NTs of a similar diameter, while in 3-layered nanotubes of similar diameters, the difference in strain energies for fluorite-type (*n*,*n*) and (*n*,0) chiralities is rather negligible. The band gaps of 6-layered titania nanotubes are found to be noticeably larger as compared to 3-layered NTs with the same diameter. When these diameters markedly increase, their band gaps asymptotically approach to those for the corresponding 2D slabs. As to other nanotube properties, the O(2*p*)–Ti(3*d*) bond hybridization is more pronounced at the projected densities of states (PDOS) calculated for equilibrium 6-layered TiO₂ NT structures, *i.e.*, they are more stable chemically.

© 2010 Elsevier B.V. All rights reserved.

1. Introduction

Titania is one of the most comprehensively studied metal oxide substances due to its widespread applications in production of catalytic, gas-sensing and corrosion-resistance materials [1]. TiO₂ attracts considerable technological interest due to the unique properties in biology, optics, electronics and photochemistry [2–4]. Recent experimental studies show that titania nanotubes (NTs) improve TiO₂ bulk properties for photocatalysis, hydrogen-sensing and photovoltaic applications [5]. TiO₂ NTs have been fabricated by a number of different methods, such as

hydrothermal treatment [6], template-assisted deposition [7,8], electro-spinning [9], and others [10]. However, the best structural stability during crystallization of titania nanotube arrays was observed in solution of H₃PO₄ and HF acids *via* simple constant-voltage experiments [1]. As a result, anatase single-crystal NTs were fabricated under suitable annealing temperature. In the X-ray diffraction (XRD) patterns of these titania nanotubes, mainly anatase phase was observed below 450° C. The rutile phase emerged in these XRD patterns near 480° C. Above this temperature, the anatase phase transformed to rutile phase gradually. In other experiments, the walls of synthesized TiO₂ NTs were identified as a polycrystalline mixture of both anatase and rutile phases [11]. Various titania nanotubes were observed in two types of morphologies: multi-walled (MW) cylindrical and scroll-like, frequently containing various types of defects and

* Corresponding author.

E-mail address: re1973@re1973.spb.edu (R.A. Evarestov).

impurities [12]. The already-synthesized MW TiO₂ NTs usually possess diameters as thin as several nanometers (nm) with inter-wall distances < 1 nm and lengths up to several micrometers (μm) [13]. Beyond the synthesis of the pure titania nanotubes there was a number of studies for titanate nanosystems, which have a high potential for applications in Li⁺ ion batteries [14], as possible precursors in the synthesis of TiO₂ NTs after thermal and chemical treatment. Layered titanate nanotubes with structures of protonic lepidocrocite H_xTi_{2-x/4}□_{x/4}O₄ (□ indicates a vacancy) [15], Na₂Ti₂O₄(OH)₂ and related alkali-containing compounds [5] as well as polytitanic H₂Ti_nO_{2n+1} acids [5,16] were synthesized. Formation mechanism of the latter was proposed to be a scrolling of the polytitanate (1 0 0) sheet along the (0 0 1) axis.

Nevertheless, despite substantial achievements in both fabrication and experimental studies of titania nanotubes, a number of theoretical studies on TiO₂ NTs was rather scarce previously [17–21], a certain progress in this area has been achieved during the last years only [22–28]. The main reason of this delay was considerable computational expenditures caused by ignorance of the rotohelical symmetry formalism, which was implemented only in recent large-scale calculations [29]. Different methods were used for theoretical simulations: empirical (molecular dynamics and mechanics), semi-empirical (tight-binding as a development of extended Hückel theory) and *ab initio* (DFT and hybrid DFT-HF implemented using formalisms of plane waves and localized orbitals). In most theoretical simulations on titania nanotubes, a schematic model 3D→2D→1D of structural transformations described in Ref. [30] was applied, *i.e.*, the bulk (3D) phase first formed a lamellar product (3D→2D) and then was bent and rolled to a nanotubular form (2D→1D). The lamellar product was mainly formed by anatase (1 0 1) surface, which is one of the most stable amongst titania slabs and was identified as prevailing in titania nanotubes [17,18,20,21,23,24]. When considering triple-layered O–Ti–O structure of sheet, the further optimization of geometry for 2D→1D transition results in formation of titania nanotubes possessing hexagonal fluorite-like (1 1 1) morphology with (*n,n*) and (*n,0*) chiralities, although details of this phase transformations were not reported so far [17,18,21]. A topology of TiO₂ nanotubes and nanotori with hexagonal morphology has been originally described recently using the formalism of graph theory [22]. In the case of 6-layered O–Ti–O–Ti–O structure, both titania sheets and the corresponding nanotubes constructed for the two possible types of nanotube chiralities, *i.e.* (*-n,n*) and (*n,n*), keep the centered rectangular anatase (1 0 1) morphology after optimization [20,23,24], which is a more realistic model as compared to the fluorite-type nanotubes. The (0 0 1) surface of the hypothetical titanium monoxide phase was also simulated for construction of the square-like morphology of Ti–O NTs, which was partially reconstructed after structural optimization [19]. In recent study [25], the authors have considered nanoribbon rutile (0 0 1) slabs for further construction of titania nanotubes. However, after optimization of the slab geometry, performed using the molecular dynamic (MD) method, they have obtained the same triple-layered O–Ti–O structure with the hexagonal fluorite-like (1 1 1) morphology. In addition to simulations on co-axial cylindrical structures for TiO₂ NTs with anatase and fluorite-type morphology [17–25] scroll-like nanostructures [18] were also considered, which were calculated using the atomic potential method as implemented in molecular mechanics (it was shown that the energetic stability of nanoscrolls grows with an increase in the number of atoms *per unit cell*). In several studies, the nanotubular structures of lepidocrocite-like titania [18,26] and titanate acids [27,28] were theoretically simulated using the semi-empirical and *ab initio* methods. The former rectangular morphology was found to be a less stable as compared to that for hexagonal fluorite-types

of TiO₂ nanotubes [18]. On the other hand, the lepidocrocite Ti_{2-x/4}□_{x/4}O₄ structures of titania sheets were theoretically simulated as spontaneously rearranged from the anatase titania (0 0 1) surface layers [31,32] and were used for large-scale *ab initio* simulations on formation of TiO₂ nanotubes [26]. All the models of titania NTs constructed so far were single-walled (SW), *i.e.*, formed from the single TiO₂ sheets.

In this paper, we focus on symmetry analysis and atomic structure as well as energetic stability and electronic properties of the stoichiometric titania (1 0 1) sheets cut from TiO₂ bulk with anatase structure, which contain either 6 (O–Ti–O–Ti–O) or 3 (O–Ti–O) layers, as well as SW nanotubes of different diameters and chiralities formed from them. So far, nobody has described TiO₂ NTs with different morphologies properly using the formalism of line groups for one-periodic (1D) nanostructures, which possess the rotohelical symmetry, as well as compared their structure and properties. There is also a lack of large-scale *ab initio* calculations on 1D-periodic models of TiO₂ NTs with full geometry optimization, using hybrid Hartree-Fock/Kohn-Sham exchange-correlation functional for proper description of their band structures. This is why some results of former studies on titania nanotubes were found to be rather incomplete and unclear. In Section 2, we consider the line group symmetry of various TiO₂ NT structures. Section 3 describes computational details used for calculations on the titania sheets and nanotubes. In Section 4, we analyze the results calculated for different TiO₂ models, systematize and discuss them. Section 5 summarizes the main conclusions obtained in this study and outlines the next steps for our further research.

2. Symmetry of TiO₂ nanotubes

The simplest description of the nanotube symmetry and structure is based on the so-called layer folding. Let **a** and **b** be the primitive translation vectors of the two-periodic (2D) lattice of the layer and γ the angle between them. The layer folding means the construction of the cylindrical surfaces of nanotubes by rolling up 2D crystalline layers. To specify the symmetry of nanotubes as monoperoic (1D) systems, it is necessary to define a finite 1D translation vector **L**=*l*₁**a**+*l*₂**b** along the nanotube axis and normal to the chiral vector **R**=*n*₁**a**+*n*₂**b** (*l*₁, *l*₂, *n*₁ and *n*₂ are integers). The nanotube of the chirality (*n*₁,*n*₂) is obtained by folding the layer in a way that the chiral vector **R** becomes circumference of the tube. The orthogonal vectors **R** and **L** are connected with the 2D lattice translation vectors **a** and **b** by the

transformation $\begin{pmatrix} \mathbf{R} \\ \mathbf{L} \end{pmatrix} = \mathbf{Q} \begin{pmatrix} \mathbf{a} \\ \mathbf{b} \end{pmatrix}$. The determinant $q = \begin{vmatrix} n_1 & n_2 \\ l_1 & l_2 \end{vmatrix}$ of

the matrix $\mathbf{Q} = \begin{pmatrix} n_1 & n_2 \\ l_1 & l_2 \end{pmatrix}$ is equal to the number of 2D lattice points in the layer supercell formed by the chiral **R** and translation **L** vectors. The orthogonality relation (**RL**)=0 can be written in the form

$$\frac{l_1}{l_2} = -\frac{n_2 a^2 + n_1 a b \cos \gamma}{n_1 b^2 + n_2 a b \cos \gamma}, \quad (1)$$

where $a = |\mathbf{a}|$ and $b = |\mathbf{b}|$. If *n* is the largest common divisor of *n*₁ and *n*₂ ($\tilde{n}_1 = n_1/n$, $\tilde{n}_2 = n_2/n$), one can introduce the reduced translation vector $\tilde{\mathbf{R}}$ along the direction of the vector **R**

$$\tilde{\mathbf{R}} = \frac{1}{n} \mathbf{R}; \quad \begin{pmatrix} \mathbf{R} \\ \mathbf{L} \end{pmatrix} = \tilde{\mathbf{Q}} \begin{pmatrix} \mathbf{a} \\ \mathbf{b} \end{pmatrix}; \quad \tilde{\mathbf{Q}} = \begin{pmatrix} \tilde{n}_1 & \tilde{n}_2 \\ l_1 & l_2 \end{pmatrix}; \quad \tilde{q} = \det(\tilde{\mathbf{Q}}) \quad (2)$$

Nanotubes, being monoperoic systems, have a line group symmetry $L=ZP$ [33,34], where *P* is the point factor and *Z* the generalized translation group. The point factor *P* is a subgroup of

an axial point group P_i belonging to one of the point symmetry groups leaving the nanotube axis invariant ($C_n, S_{2n}, C_{nv}, C_{nh}, D_n, D_{nd}, D_{nh}$). The line group can be factorized also as $L=TP_i$, where T is the subgroup of the pure translations along the nanotube axis. Such a factorization is traditional in crystallography and it is accepted for the monoprotic rod groups [35] being a particular case of line groups for $m=1, 2, 3, 4, 6$. The group Z is infinite and cyclic, describing either the glide plane reflections $T'=(\sigma_v|\frac{1}{2})$ or the screw axis rotations by $2\pi/n\tilde{q}$ (for $\tilde{q} > 1$) generated by helical operations $T_q^r=(C_q^r|1/\tilde{q})$, where r -integer. For $n > 1$, pure rotations appear and form subgroup of point symmetry group P . The smallest helical vector \mathbf{H} is defined as $\mathbf{H}=h_1\mathbf{a}+h_2\mathbf{b}=(r/n\tilde{q})\mathbf{R}+(1/\tilde{q})\mathbf{L}$ and satisfies the following conditions: $\tilde{n}_1h_2-\tilde{n}_2h_1=1; h_1l_2-h_2l_1=r$. The projections of the helical vector \mathbf{H} on the chiral vector \mathbf{R} and translation vector \mathbf{L} (Fig. 1a) define the rotational and translational parts of helical rotation T_q^r , respectively.

The symmetry of nanotube is defined by: (i) nanotube chirality (n_1, n_2) , (ii) translation vector components (l_1, l_2) found from the orthogonality relation, Eq. (2), (iii) point symmetry of the rolled 2D lattice (see later). The orthogonality relation has different forms for different 2D lattices:

- rectangular primitive ($\cos \gamma=0; a \neq b$):

$$\frac{l_1}{l_2} = -\frac{n_2a^2}{n_1b^2}, \text{ or } l_1n_1b^2 = -l_2n_2a^2; \quad (3a)$$

- rectangular centered ($\cos \gamma \neq 0, 0.5; a=b$):

$$\frac{l_1}{l_2} = -\frac{n_2+n_1\cos \gamma}{n_1+n_2\cos \gamma}; \quad (3b)$$

- square ($\cos \gamma=0; a=b$):

$$\frac{l_1}{l_2} = -\frac{n_2}{n_1}, \text{ or } l_1n_1+l_2n_2=0; \quad (3c)$$

- hexagonal ($\cos \gamma=0.5; a=b$):

$$\frac{l_1}{l_2} = -\frac{2n_2+n_1}{2n_1+n_2}. \quad (3d)$$

It is well seen from Eq. (3) that the translational symmetry of the nanotube may exist for any arbitrary chirality (n_1, n_2) if the nanotube is obtained by folding the layer with square or hexagonal 2D lattices. However, there are restrictions on the possible chiralities for rectangular lattices: $(n, 0), (0, n)$ for rectangular primitive and $(-n, n), (n, n)$ for rectangular centered ones.

There are known 13 families of line groups [33]: each family includes all groups (with various parameters $n, r/q$ and partial translation $f=1/\tilde{q}$) with fixed types of Z group and P factor. The translations of the layer become rotohelical operations T_q^r on the nanotube, giving the first family subgroup $L^{(1)}=ZP$ ($P=C_n$) of the nanotube line group L . The latter has the same parameters for the ray of the nanotubes $(n_1, n_2)=n(\tilde{n}_1, \tilde{n}_2)$, differing by n .

Apart from the translational invariance, 2D lattice has rotational C_2 symmetry generated by the rotation of π around the axis perpendicular to the layer. For the square and hexagonal lattices, the order of this rotational axis is higher: 4 and 6, respectively. Whenever the order of the principal axis of the layer is 2, 4 or 6, the symmetry of the nanotube is the fifth family line group at least $L^{(5)}=ZP$ ($P=D_n$).

In addition, the non-oblique 2D lattices have both vertical mirror and glide planes. In the layer groups some of the 2D lattice symmetry operations are absent. The symmetry operation matrices $G^{(3)}=(F^{(3)}|\mathbf{t}^{(2)})$, corresponding to the layer group, consist of orthogonal $F^{(3)}$ and translational $\mathbf{t}^{(2)}$ parts. Let the Cartesian axes x, y and z to be directed along the chiral vector \mathbf{R} , the nanotube translation vector \mathbf{L} and the layer principal axis

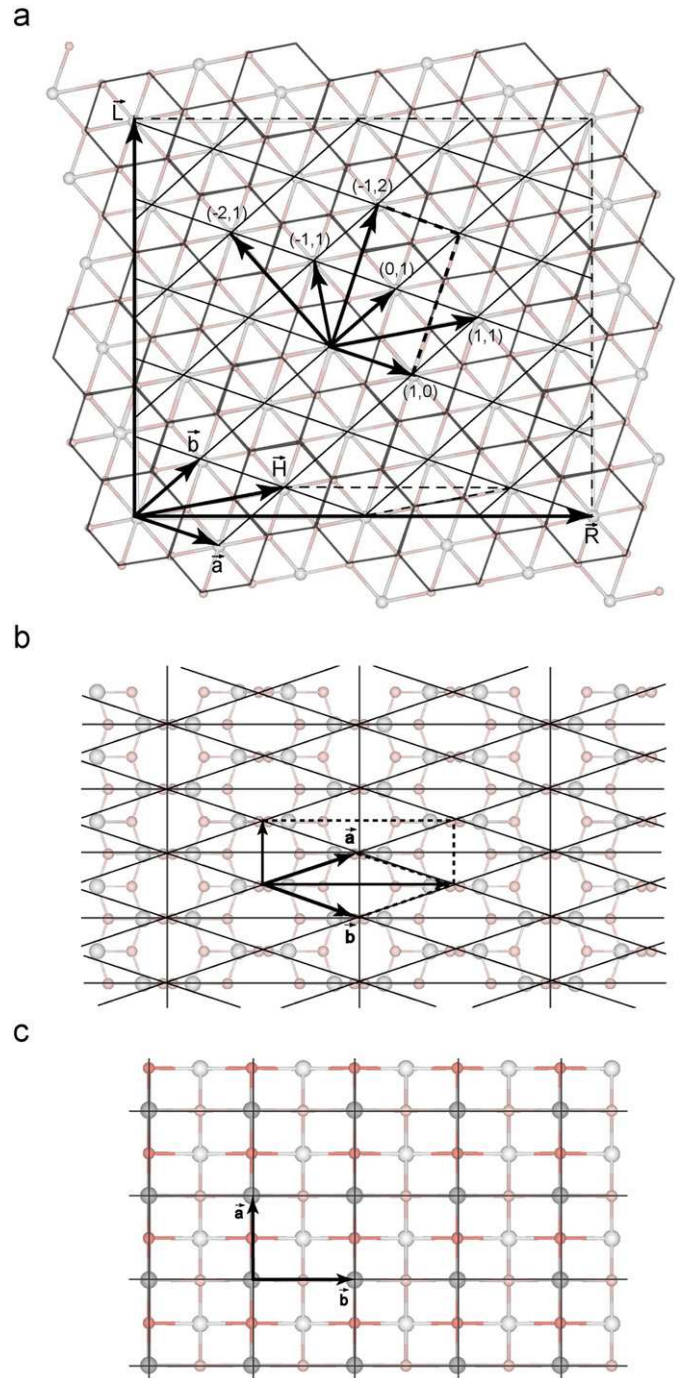


Fig. 1. The ways of construction of a single-walled nanotubes via the primitive translation vectors \mathbf{a} and \mathbf{b} as well as arbitrary translation (\mathbf{L}) and chiral (\mathbf{R}) vectors for three types of titania sheets: (a) 3-layered hexagonal (fluorite) slab (the reduced chirality vectors $(\tilde{n}_1, \tilde{n}_2)$ are shown here for $\tilde{n}_1=0, \pm 1$ and $\tilde{n}_2=1, 2$), (b) 6-layered centered rectangular (anatase) slab, (c) 6-layered primitive rectangular (lepidocrocite) slab.

perpendicular to the layer, respectively. During the folding procedure after transformation described by Eq. (1) of 2D lattice the orthogonal symmetry operations survive if they do not change the z coordinate (the layer is rolled up to the tube) and do not mix or interchange x and y coordinates (chirality and translation vectors are supposed to be fixed). It means that after folding the layer, only those layer group symmetry operations survive, which

had the diagonal 2×2 submatrices $\mathbf{F}^Q = \begin{pmatrix} \pm 1 & 0 \\ 0 & \pm 1 \end{pmatrix}$:

$$\mathbf{E} = \begin{pmatrix} 1 & 0 \\ 0 & 1 \end{pmatrix}, \quad \mathbf{U} = \begin{pmatrix} -1 & 0 \\ 0 & -1 \end{pmatrix}, \quad \sigma_v = \begin{pmatrix} -1 & 0 \\ 0 & 1 \end{pmatrix}, \quad \sigma_h = \begin{pmatrix} 1 & 0 \\ 0 & -1 \end{pmatrix} \quad (4)$$

The transformations (4) include the rotation U by π around the second-order axis, normal to the tube, and reflections in planes, orthogonal to the 2D lattice plane and parallel to the tube axis, directed along translation vector \mathbf{L} (σ_v) or orthogonal to it (σ_h). The transformed translations \mathbf{t}^Q can be written in the components of vectors \mathbf{R} and \mathbf{L} as

$$\mathbf{t}^Q = (0 \ 0), \quad \left(\frac{1}{2n} \ 0\right), \quad \left(0 \ \frac{1}{2}\right), \quad \left(\frac{1}{2n} \ \frac{1}{2}\right), \quad (5)$$

where $n=1$ for the reduced chirality vector $\hat{\mathbf{R}}$ while $1/2$ in the second position produces the non-symmorphic line groups containing helical rotation $T_{2n}^1 = (C_{2n}^1 | \frac{1}{2})$ or the reflection in glide plane $T' = (\sigma_v | \frac{1}{2})$. The nanotube symmetry groups are formed by the point symmetry operations (4) and translations (5) survived after folding and combined in such a way that they form the line group $L=ZP$ (the line groups of families 2–13) [34]. The procedure described may be applied to find the nanotube symmetry if the symmetry of the layer group used for folding is known.

We applied this approach to analyze the symmetry of TiO_2 nanotubes. In the former TiO_2 nanotube calculations there were used three different models: $3an$ (1 0 1)—the anatase (1 0 1) slab consists of the 3 atomic layers [17,18,21], $6an$ (1 0 1)—the anatase (1 0 1) slab consists of the 6 atomic layers [20,23,24] and the 6-layered lepidocrocite-like TiO_2 (0 1 0) slab [18,26]. The model of lepidocrocite was built from the unit cell of $\text{FeO}(\text{OH})$ by exchanging the Fe atoms to titaniums, omitting the hydrogen atoms and cutting a slab in the (0 1 0) direction in the plane between the formerly hydrogen-bonded sheets [26]. The models $3an$ (1 0 1), $6an$ (1 0 1) and $6lep$ (0 1 0) are shown in Figs. 1a–c, respectively.

The diperiodic (layer) groups for each model were found by the following way. The 3- or 6-plane slabs were cut out from the bulk crystals of anatase (tetragonal space group $I4_1/amd$) and lepidocrocite (orthorhombic space group $Cmcm$). For all the three models, the 3D space groups were found by adding to the 2D slab lattice the translation vector orthogonal to it and using the FINDSYM code [35], which identifies the 3D space group of a crystal and gives the Wyckoff positions of the atoms in a unit cell. To find the layer groups for each model, the mapping between the three-periodic 3D space groups and diperiodic 2D layer groups was used [36]. Both nanotube chiralities and corresponding line group families compatible with NT periodicity were determined from Table 1 from Ref. [34]. After folding of anatase layers the reflections σ_v or σ_h survive and combine with helical rotations. In the case of lepidocrocite layers U , σ_v and σ_v operations provide the

point group D_{nh} . The information about the symmetry of these models is given in Table 1.

3. Computational details

The first principles linear combination of atomic orbitals (LCAO) calculations of various titania sheets and nanotubes have been performed using the hybrid HF-KS (PBE0) exchange-correlation functional [37]. The small-core pseudopotential [38] of Ti atom is used in these calculations (3s, 3p, 3d and 4s-electrons were taken as valence electrons), while the all-electron triple-zeta (TZ) quality basis set (BS) for O-atom has been taken from Ref. [39]. It is well known that in the LCAO calculations of crystals BS of free atom has to be modified as the diffuse functions cause numerical problems because of the large overlap with the core functions of the neighboring atoms in a densely packed crystal [40]. There exist a number of different algorithms for minimization of many variables function [41]. The comparative study of their efficiency for the basis set optimization in crystals has been performed recently [42].

To optimize the BS in present study, we use the minimization method without calculations on the total energy derivatives developed by Powell [43] often called 'the method of conjugate directions'. It is estimated as one of the most efficient direct minimization methods. Being interfaced with the CRYSTAL06 LCAO computational code [44] our program package OPTBAS [42] has been applied for the BS optimization. The BS exponential parameters less than 0.1 were excluded from the AOs and the bound-constrained optimization has been performed for the remaining exponential parameters with a 0.1 lower bound. As a result, for the titanium BS, we have excluded the most diffuse exponents 0.08558, 0.03330 and 0.07200 optimizing all the other external exponents and obtaining 0.6162147 for s , 0.353023 for p as well as 0.8769347 and 0.3384701 for the last two d shells (cf. 0.5128, 0.39820, 0.8002 and 0.2620 [38], respectively). For the oxygen BS, nothing has been excluded while the three outer exponents have been re-optimized, i.e., for the last two sp shells we have obtained 0.9033819 and 0.2576692 as well as 0.2584551 for d shell (cf. 0.905661, 0.255611 and 1.292 [39], respectively).

The diffuse exponents of valence s , p and d orbitals have been optimized for anatase phase of bulk titania. Its atomic and electronic properties have been reproduced in a good agreement with the experiment (the experimental values are given in brackets): the lattice parameters $a=3.784 \text{ \AA}$ (3.782 \AA) and $c=9.508 \text{ \AA}$ (9.502 \AA), the dimensionless parameter for relative position of oxygen atom $u=0.2074$ (0.2080), as well as the band gap $\Delta\varepsilon_{\text{gap}}=4.0 \text{ eV}$ (3.2 eV). These results for the bulk anatase agree with the experimental data better than those given in Ref. [45] for both plane wave (PW) and LCAO calculations when using the different exchange-correlation potentials. Although certain

Table 1
The symmetry properties of TiO_2 nanotubes.

NT model	2D lattice	Diperiodic group	Chiralities	Family	Line group	P_i	N_a^a
$3an$ (1 0 1)	Hexagonal	72 $P\bar{3}m1$	$(n,n), (-n,2n), (-2n,n)$	4 $T_{2n}^1 C_{nh}$	$(2n)_n/m$	C_{2nh}	$6n$
			$(n,0), (0,n), (-n,n)$	8 $T_{2n}^1 C_{nv}$	$(2n)_n/mc$	C_{2nv}	$6n$
$6an$ (1 0 1)	centered rectangular	18 $C2/m11$	$(-n,n)$	4 $T_{2n}^1 C_{nh}$	$(2n)_n/m$	C_{2nh}	$12n$
			(n,n)	8 $T_{2n}^1 C_{nv}$	$(2n)_n/mc$	C_{2nv}	$12n$
$6lep$ (0 1 0)	primitive rectangular	46 $Pmmn$	$(n,0), (0,n)$	11 $T D_{nh}$	n/mmm^b $(\bar{2}n)2m^c$	D_{nh}	$6n$

^a Number of atoms per nanotube unit cell.

^b For even n .

^c For odd n .

improvement of substantially underestimated values of $\Delta\epsilon_{\text{gap}}$ for bulk anatase in the DFT PW calculations was achieved recently [25] when using the LDA+ U method (2.7 eV).

The SW NT monoperoic translation symmetry is adopted for our nanotube calculations as it is implemented with POLYMER option in CRYSTAL06 code [44]. Unfortunately, this option takes into account only the symmetry of rod groups being the subset of the nanotube line groups as present in Table 1. On the other hand, the LCAO method, which is implemented in the CRYSTAL06 code, allows one to describe both *single* 1D nanotubes and 2D sheets, unlike the PW method, which is more widespread for calculations on low-dimensional periodic systems. Indeed, to restore the 3D periodicity in the PW nanotube calculations, the NT supercell is artificially introduced: the nanotubes are placed into a square array with the inter-tube distance equal to 10–30 Å. At such separations the NT–NT interaction is usually found to be rather small, for example, when increasing the inter-distance between the SW carbon nanotubes with armchair chirality (3,3) from 10 to

20 Å, the calculated change in the work function was found to be only 0.003 eV [46]. However, the convergence of results obtained using PW calculations depends on the artificial inter-tube interactions; thus, the additional computational efforts should be provided to ensure their negligibility. This artefact is certainly absent in our LCAO nanotube calculations.

4. Results and discussion

4.1. TiO_2 slabs of different thicknesses with initial anatase (1 0 1) structure

2D titania sheets, which have been considered in Section 2 as species rolled to a nanotubular form (2D→1D), have a thickness of a few atomic layers. In spite of their low dimensionality these sheets were found to be remarkably stable [32]. The anatase (1 0 1) surface exposes five- and six-fold coordinated titanium atoms, as well as two- and three-fold coordinated oxygen atoms (Fig. 2). As a result, the (1 0 1) surface is found to be much more stable than the (0 0 1) one [47] (the latter can be easily reconstructed to a surface with lepidocrocite structure as observed earlier [31,32]). Because the (1 0 1) film can be easier organized in double subsheets consisting of the two formula units, *i.e.*, 6-layered O–Ti–O–Ti–O slabs (Fig. 2b), it makes sense to consider mainly sheets made of an even number of layers. However, theoretical simulations on TiO_2 sheets and nanotubes originated from the 3-layered O–Ti–O slabs (Fig. 2a) as a more simple system for numerical simulations [17,18,21]. In the present study, we have optimized the structures of 3-, 6- and 12-layered anatase (1 0 1) slabs (from those corresponding to anatase bulk) as well as calculated their properties. Mulliken population analysis was used to estimate the atomic effective charges. Main results obtained for these slabs compared with the corresponding bulk properties of titania anatase phase are present in Table 2. To compare the energies of n -layered sheets, we define both formation energy (E_{form}) *per* TiO_2 formula unit and surface energy (E_{surf}) *per* area of primitive surface cell

$$E_{\text{form}}(n) = \left(\frac{E_n}{n} - E_b \right), \quad (6a)$$

$$E_{\text{surf}}(n) = \frac{1}{2S} (E_n - nE_b), \quad (6b)$$

where E_n is the total n -layered slab energy *per* primitive surface unit cell and S its area while E_b is the total energy *per* primitive bulk unit cell. The relaxation energy E_{relax} is a difference between the total energies of slabs *before* and *after* relaxation *per* TiO_2 formula unit.

We have found that the structural optimization of the 3an (1 0 1) slab results in a spontaneous (barrier-less) reconstruction

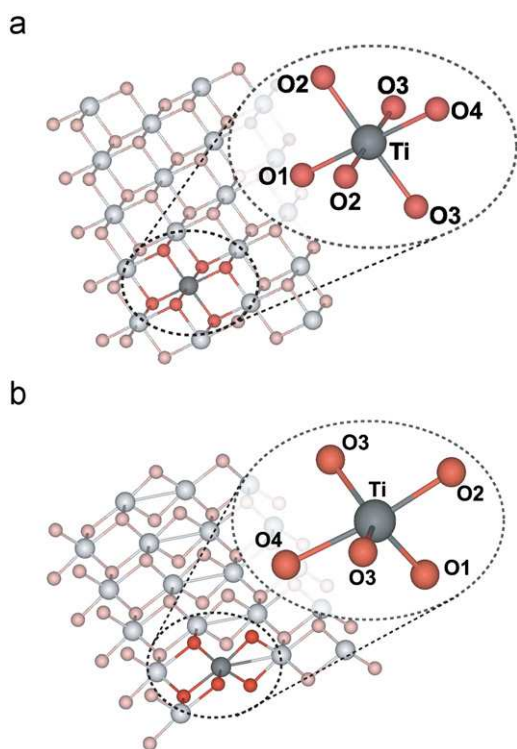


Fig. 2. Two different types of coordination for Ti atoms in: (a) 3-layered hexagonal titania sheets (six-fold) and (b) 6-layered centered rectangular titania sheets (five-fold).

Table 2

The structural and electronic properties of optimized titania slabs and bulk.

Models of TiO_2 sheets and bulk	Lattice parameters (Å)		Thickness (Å)	Bond length $d_{\text{Ti-O}}^a$ (Å)				Mulliken charge, q_{Ti}^b (e)	Various energies			
	a	c		Ti–O1	Ti–O2	Ti–O3	Ti–O4		E_{relax} (eV/ TiO_2)	E_{form} (eV/ TiO_2)	E_{surf} (J/m ²)	$\Delta\epsilon_{\text{gap}}^c$ (eV)
3-layered (1 1 1) ^d	2.96	–	1.92	1.95	1.96	1.97	1.98	2.45	–6.05	0.49	0.44	4.89
6-layered (1 0 1)	3.51	5.45	2.39	1.75	1.89	1.91	2.05	2.28	–1.09	0.74	0.64	5.14
12-layered (1 0 1)	3.71	5.46	5.83	1.77	1.83	1.95	2.01	2.30	–0.55	0.43	0.67	4.92
Bulk ^e	3.78	9.51	–	1.935	1.935	1.973	1.973	2.35	–	–	–	4.09

^a The corresponding bonds are shown in Fig. 2.

^b Averaged effective charges q_{O} are as twice as smaller than q_{Ti} , with opposite sign.

^c All band gaps considered in this Table are indirect.

^d Properties calculated for this slab with hexagonal structure differ from those for 6- and 12-layered anatase slabs.

^e BSs have been optimized for TiO_2 bulk and neither its relaxation nor surface properties can be present here.

to the hexagonal (111) fluorite structure (instability of the former as compared to the latter is well illustrated by large relaxation energy: -6.05 eV per formula unit). This structure

(Fig. 3a) can really exist in a metastable phase of bulk titania under extremely high pressure [48]. In previous papers about simulation on 3-layered TiO₂ NTs [17,18,21,22], nothing

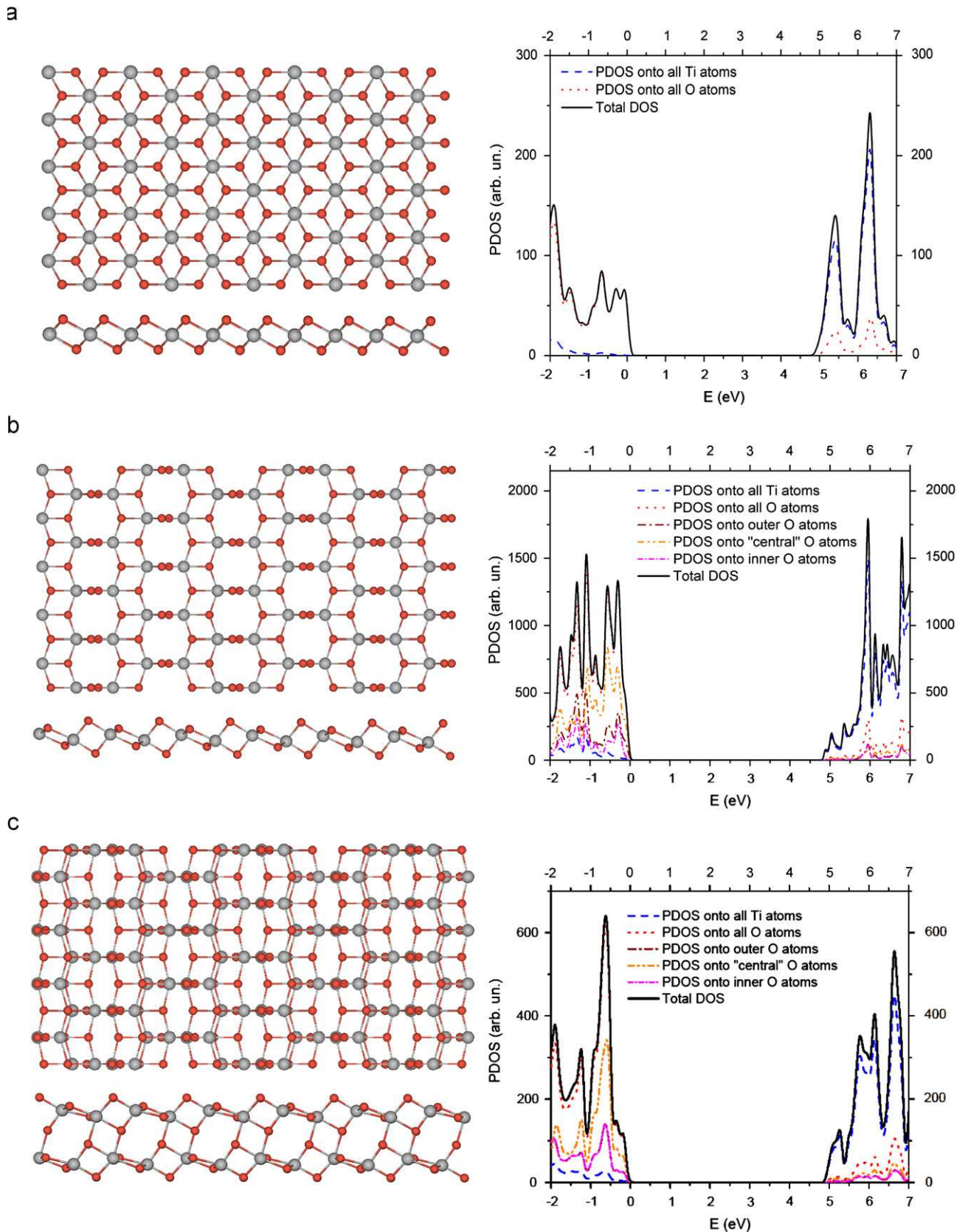


Fig. 3. Atop and across views of titania sheets as well as their total and projected DOS for: (a) 3-layered slab, (b) 6-layered slab and (c) 12-layered slab.

was mentioned on this structural reconstruction, the authors simply considered hexagonal structures of nanotubes as initial ones. Only in recent paper [25], the authors analyzed structural reconstruction from the double-layered rutile (0 0 1) slab to the 3-layered fluorite (1 1 1) slab and then considered the corresponding O–Ti–O nanotubes. Both 6- and 12-layered anatase (1 0 1) slabs (Fig. 3b,c) keep the same symmetry after optimization, while the lattice parameters differ from those in bulk. Relaxation energy in both cases is markedly smaller as compared to 3-layered TiO₂ slab (Table 2). Surface and formation energies of three titania slabs are qualitatively similar to those calculated earlier [25,32,47]: the former grow on increasing the thickness of the slab, and the latter reduce. Since the optimized 3-layered slab has a hexagonal structure its parameters cannot be compared directly with those for the 6- and 12-layered slabs, whose structure is rectangular centered.

As to a band gap of titania, it was found indirect for all three slabs and bulk. When comparing $\Delta\epsilon_{\text{gap}}$ for 6- and 12-layered slabs (Table 2) we can conclude that on increasing the thickness of titania sheet the band gap should approach the value of anatase bulk. At the same time, $\Delta\epsilon_{\text{gap}}$ for 3-layered slab describes the

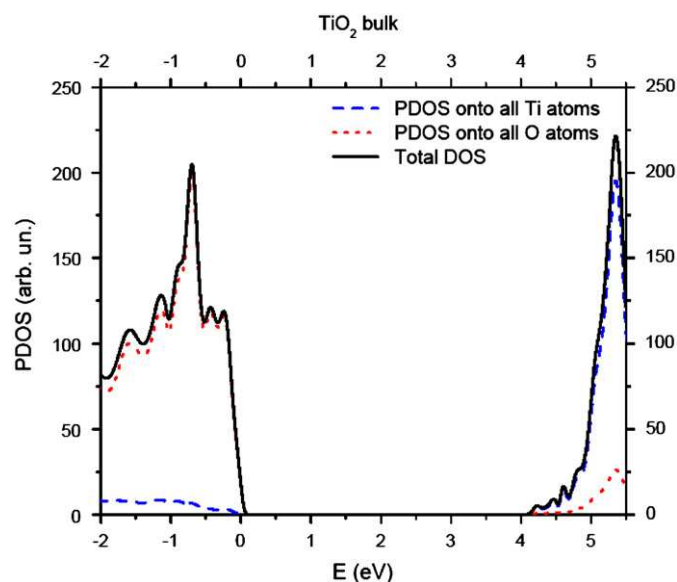


Fig. 4. The total and projected DOS for TiO₂ bulk (anatase phase).

Table 3

The structural and electronic properties of the optimized 3-layered titania nanotubes.

NT chirality indices	N_a	l_{NT} (Å)	D_{NT} (Å) ^a	h_{NT} (Å)	$d_{\text{Ti-O}}$ (Å)				q_{Ti} (e)	E_{relax} (eV/TiO ₂)	E_{strain} (eV/TiO ₂)	$\Delta\epsilon_{\text{gap}}$ (eV) ^b
					Ti–O1	Ti–O2	Ti–O3	Ti–O4				
<i>(n,n) nanotubes</i>												
(6,6)	36	2.99	10.06	1.86	1.89	1.94	2.00	2.05	2.42	−0.09	0.479	4.66 ⁽ⁱ⁾
(9,9)	54	2.98	14.88	1.89	1.91	1.94	1.99	2.02	2.43	−0.05	0.208	4.74 ⁽ⁱ⁾
(12,12)	72	2.97	19.73	1.91	1.935	1.95	1.98	1.995	2.44	−0.04	0.117	4.77 ⁽ⁱ⁾
(15,15)	90	2.97	24.61	1.91	1.94	1.95	1.98	1.99	2.45	−0.04	0.075	4.79 ⁽ⁱ⁾
(18,18)	108	2.97	29.51	1.91	1.945	1.955	1.97	1.98	2.45	−0.03	0.052	4.80 ⁽ⁱ⁾
<i>(n,0) nanotubes</i>												
(8,0)	48	5.065	8.17	1.83	1.89	1.94	1.955	2.135	2.40	−0.33	0.792	4.65 ⁽ⁱ⁾
(12,0)	72	5.095	11.70	1.88	1.915	1.945	1.96	2.03	2.43	−0.09	0.349	4.70 ⁽ⁱ⁾
(18,0)	108	5.115	17.23	1.90	1.935	1.95	1.965	1.965	2.44	−0.05	0.155	4.75 ⁽ⁱ⁾
(24,0)	144	5.12	22.88	1.91	1.94	1.95	1.97	1.985	2.45	−0.04	0.089	4.79 ^(d)
(30,0)	180	5.125	28.55	1.92	1.945	1.955	1.975	1.98	2.45	−0.04	0.057	4.82 ^(d)

^a Diameters are given for the middle cylinders between the external and internal walls of nanotubes.

^b Direct and indirect band gaps marked by superscript indices ^(d) and ⁽ⁱ⁾, respectively.

corresponding electronic property of another, fluorite titania phase. The total and projected densities of states (DOS and PDOS) for both titania bulk and sheets are shown in Figs. 3 and 4. A certain correlation between the DOSs of anatase slabs (Fig. 3b,c) and bulk (Fig. 4) confirms the conclusion made earlier for the corresponding band gaps.

4.2. Three-layered single-walled TiO₂ nanotubes with hexagonal structure

In Table 3, we compare results obtained after structural optimization of 3-layered titania NTs with (i) armchair-like (n,n) chirality (for $n=6, 8, 12, 15, 18$) and (ii) zigzag-like ($n,0$) chirality (for $n=8, 12, 18, 24, 30$). The optimized structures of the four selected nanotubes of both chiralities (the two NT models *per* each chirality) are shown in Fig. 5. One of the main parameters of nanotube stability, *i.e.*, the strain energy E_{strain} , is defined as a difference between the total energies of the optimized nanotube (E_{NT}) and the corresponding slab before rolling up (E_{slab}), taking into account the number k of slab unit cells in nanotube unit cell containing m formula units TiO₂ (all energy parameters are present in eV)

$$E_{\text{strain}} = \frac{1}{m}(E_{\text{NT}} - kE_{\text{slab}}). \quad (7)$$

We also compare in Table 3 the numbers of atoms *per* NT unit cell (N_a), the optimized length of NT translational vector (l_{NT}), diameters of nanotubes (D_{NT}) and their thicknesses (h_{NT}), Ti–O bond lengths ($d_{\text{Ti-O}}$), effective atomic charges as on titanium atoms (q_{Ti}), relaxation energies (E_{relax}) and band gaps ($\Delta\epsilon_{\text{gap}}$). The relaxation energy E_{relax} for nanotubes is a difference between the total energies of non-relaxed NTs rolled up from the slabs with optimized structure and those after relaxation *per* TiO₂ formula unit. Some of these results may be directly compared with the corresponding values calculated by us for the 3-layered titania slabs (Table 2) and the 6-layered nanotubes (Table 4).

Obviously, the number of atoms *per* surface unit in ($n,0$) nanotubes is markedly larger than that in (n,n) NTs of the same diameter; thus, the latter can be calculated faster. For a small D_{NT} (low chirality indices), the absolute values of both E_{relax} and E_{strain} are large enough, and trying to reduce these diameters even more, we face an enhanced instability of NTs. For example, the convergence of calculations on (4,4) and (6,0) nanotubes has been found to be rather poor. Since hypothetical nanotubes with infinite diameter should coincide with sheets of the same thickness, a consequent growth of the NT diameters leads to a

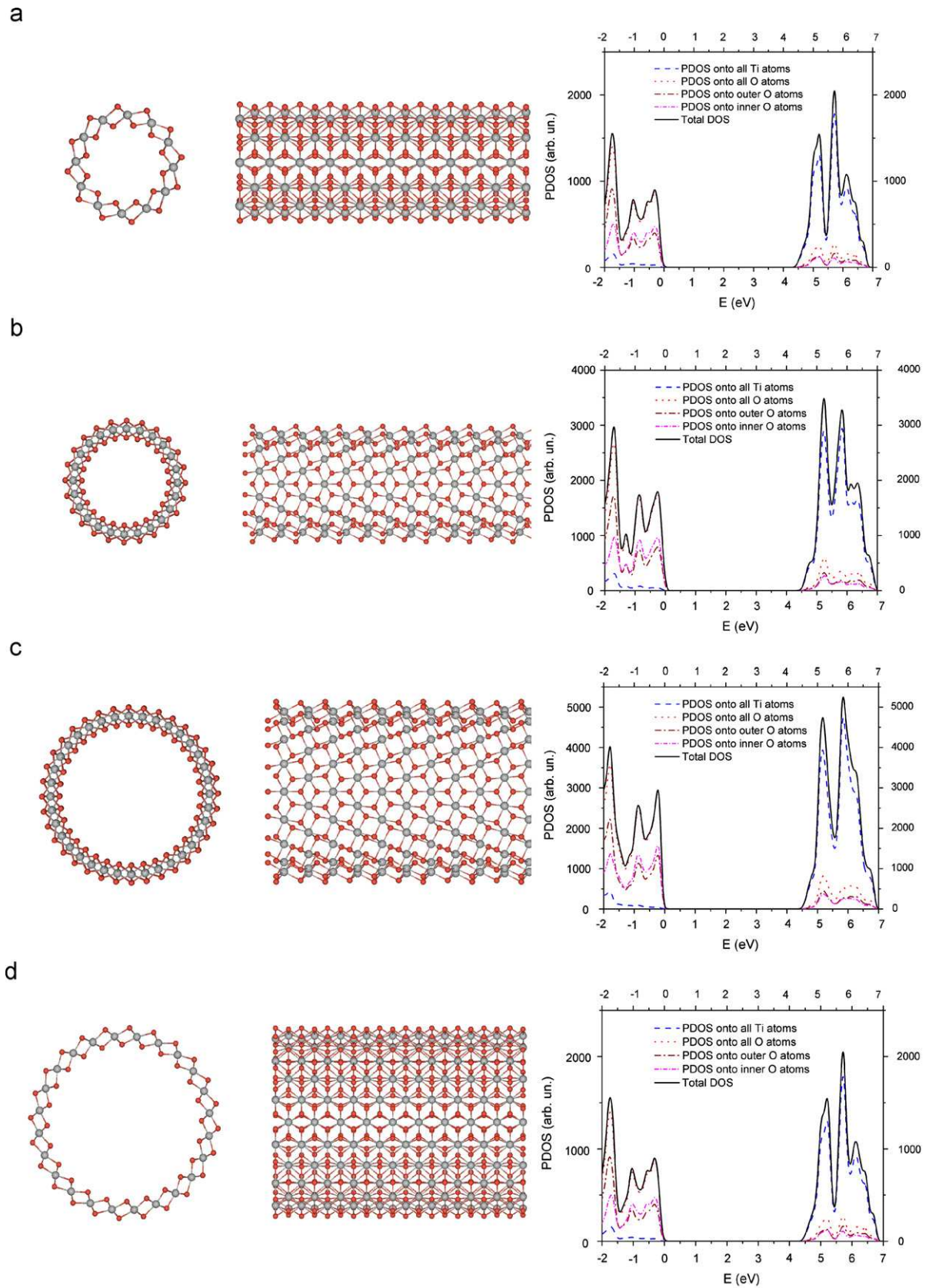


Fig. 5. Atop and cross views of 3-layered TiO₂ NTs as well as their total and projected DOSs for different chiralities: (a) (6,6), (b) (12,0), (c) (18,0) and (d) (12,12).

substantial decrease in both relaxation and strain energies (down to zero at infinity), whereas the values of l_{NT} , h_{NT} , d_{Ti-O} , q_{Ti} and $\Delta\epsilon_{gap}$ (Table 3) approach to those for 3-layered titania slab with a

hexagonal structure (Table 2). All the band gaps of nanotubes with (n,n) chirality presented in Table 3 are indirect, but this is not true for $(n,0)$ chirality. The total and projected densities of states

Table 4
The structural and electronic properties of the optimized 6-layered titania nanotubes.

NT chirality indices	N_a	l_{NT} (Å)	D_{NT} (Å) ^a	h_{NT} (Å)	d_{Ti-O} (Å)				q_{Ti} (e)	E_{relax} (eV/TiO ₂)	E_{strain} (eV/TiO ₂)	$\Delta\epsilon_{gap}$ (eV) ^b
					Ti–O1	Ti–O2	Ti–O3	Ti–O4				
<i>(-n,n) nanotubes</i>												
(-3,3)	36	3.66	9.98	2.45	1.795	1.86	1.925	2.025	2.28	-0.82	0.175	4.92 ⁽ⁱ⁾
(-4,4)	48	3.60	13.30	2.41	1.775	1.89	1.94	2.01	2.21	-0.35	0.126	5.40 ⁽ⁱ⁾
(-6,6)	72	3.54	19.84	2.39	1.765	1.87	1.92	2.11	2.19	-0.14	0.067	5.26 ⁽ⁱ⁾
(-9,9)	108	3.52	29.68	2.39	1.77	1.875	1.91	2.09	2.27	-0.05	0.047	5.19 ⁽ⁱ⁾
(-12,12)	144	3.52	39.55	2.39	1.77	1.88	1.90	2.085	2.27	-0.03	0.033	5.17 ⁽ⁱ⁾
<i>(n,n) nanotubes</i>												
(6,6)	72	10.32	7.22	2.44	1.79	1.835	1.96	2.01	2.27	-1.68	0.358	4.76 ^(d)
(10,10)	120	10.39	11.85	2.46	1.80	1.835	1.945	2.02	2.27	-0.45	0.191	5.05 ^(d)
(15,15)	180	10.33	17.33	2.43	1.785	1.87	1.92	2.01	2.27	-0.14	0.127	5.36 ⁽ⁱ⁾
(20,20)	240	10.33	22.84	2.41	1.78	1.875	1.91	2.01	2.28	-0.07	0.088	5.28 ^(d)
(24,24)	288	10.33	27.24	2.41	1.78	1.875	1.895	2.01	2.28	-0.03	0.068	5.24 ^(d)

^a Diameters are given for the middle cylinders between the external and internal walls of nanotubes.

^b Direct and indirect band gaps marked by superscript indices ^(d) and ⁽ⁱ⁾, respectively.

for the selected 3-layered NT models are shown in Fig. 5. A more detailed comparative analysis of these properties and their verification are present in Section 4.4.

4.3. Six-layered single-walled TiO₂ nanotubes with centered rectangular structure

In Table 4, we present results obtained after structural optimization of 6-layered TiO₂ NTs with (i) $(-n,n)$ chirality (for $n=3, 4, 6, 9, 12$) and (ii) (n,n) chirality (for $n=6, 10, 15, 20, 24$). Analogously to Fig. 5, we show in Fig. 6 the optimized structures of the four selected 6-layered nanotubes of both chiralities, whose diameters are very close to those for the corresponding 3-layered NTs (Table 5). Definition of values presented in Table 4 is the same as before in Table 3.

A specific feature of the 6-layered titania sheets and nanotubes with anatase structure is that both Ti sublayers are rearranged in the middle between both the surfaces of sheets and nanotubes (Figs. 3b and 6), i.e., their formal structure is O₂-Ti-Ti-O₂ and not O-Ti-O₂-Ti-O as written previously according to a sequence of TiO₂ formula units in the bulk anatase structure. However, the middle of 12-layered TiO₂ slab, considered in Section 4.1 too, consists of two sublayers containing oxygen atoms (Fig. 3c), and when we obtain the single-walled titania nanotube by rolling up this 12-layered sheet its thickness is about 2.5 times larger than that for 6-layered TiO₂ nanotube. As a result, the atomic structure of the internal circumference of this 12-layered NT is overstrained even for moderate values of D_{NT} and convergence during its test optimization has been found to be rather poor. Thus, we can predict that for 12-layered titania nanotube, the more preferable morphology has to be not SW, but the double-wall (DW) NT consisting of a pair of 6-layered nanotubes of different diameters and chirality indices.

Each Ti atom in the 6-layered titania sheets and nanotubes exposes the five-fold coordination with adjacent oxygen atoms not the six-fold one as in both anatase bulk and 3-layered fluorite-type (1 1 1) sheets and nanotubes (Fig. 2). As a result, we observe noticeable differences between the calculated properties of 3- and 6-layered sheets and nanotubes (Tables 2–4). First of all, the strain energies of the 6-layered nanotubes are smaller than those of the 3-layered NTs of close diameters (for $D_{NT} \leq 20$ – 25 Å) while the relaxation energies of the former are larger (especially for small D_{NT}), due to a more complicated morphology (Fig. 6). Moreover, unlike 3-layered NTs, the values of d_{Ti-O} for the internal circumference (Ti–O1 bonds) for

6-layered NTs are noticeably compressed. The band gaps of 6-layered sheets and nanotubes are larger too, by 0.25–0.45 eV (depending on D_{NT}). For the $(-n,n)$ chirality, these gaps are always indirect while for (n,n) one they are mainly direct. The total and projected densities of states for the selected 6-layered NT models are shown in Fig. 6.

4.4. Comparison of the structural and electronic properties of single-walled TiO₂ nanotubes

In Table 5, we compare results of calculations on four pairs of structurally close TiO₂ nanotubes shown in Figs. 5 and 6. The optimized values of D_{NT} in each pair of these NTs have been selected very close (relative difference of the diameters in different pairs has varied from 0.57% to 1.34%). Structural compatibility of all four pairs can be explained by their belonging to the same line groups (Table 1), i.e., chiralities of 3-layered (n,n) and 6-layered $(-n,n)$ nanotubes can be described by the same line group $(2n)_n/m$, whereas the line group $(2n)_nmc$ corresponds to both 3-layered $(n,0)$ and 6-layered (n,n) NTs. Parallel with the proximity of diameters, this symmetry factor makes reasonable the direct comparison of the structural and electronic properties in each pair of these nanotubes.

We can conclude from the data presented in Table 5 that in 3- and 6-layered nanotubes with close diameters described by $(2n)_n/m$ symmetry group, the number of atoms per unit cells is the same whereas the length of unit cell of the latter is about 20% larger. In the analogous NT pairs described by $(2n)_nmc$ symmetry group the number of atoms per unit cells is larger by about 70% for 6-layered nanotubes, while their lengths are more than twice as larger as compared to 3-layered NTs. Thus, if we estimate the density of atoms per NT length, it will be larger for 3-layered nanotubes. 6-layered NT thickness is by $\sim 30\%$ larger than that in 3-layered nanotubes for all chiralities. As to Ti–O bond lengths, their deformation is noticeably larger in 6-layered nanotubes, and it is not decreased for D_{NT} up to 30 Å, whereas in 3-layered NTs, values of d_{Ti-O} approach to those in 3-layered slab (Table 2) much faster. Obviously, this is also true for convergence of E_{relax} with D_{NT} increasing (Table 5).

We also analyze E_{strain} and $\Delta\epsilon_{gap}$ dependence on D_{NT} for all four sets of 3- and 6-layered TiO₂ NTs simulated in present study (Figs. 7 and 8, respectively). We consider large enough range of nanotube diameters, from 0.5 to 4.0 nm, with a number of atoms per NT unit cell increased from 30 up to 288. To construct both plots in Figs. 7 and 8, we have performed

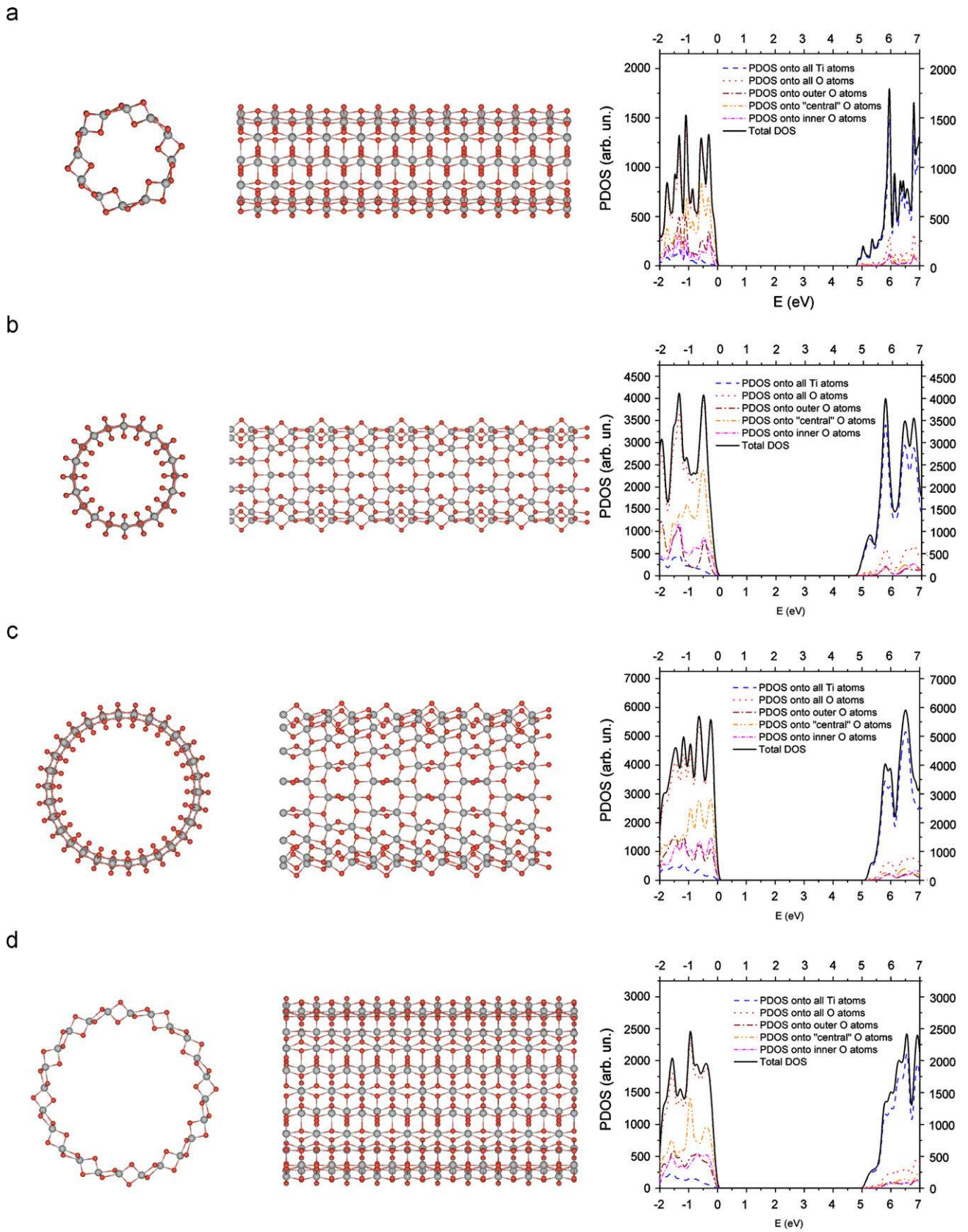


Fig. 6. Atop and across views of 6-layered TiO₂ NTs as well as their total and projected DOSs for different chiralities: (a) (-3,3), (b) (10,10), (c) (15,15) and (d) (-6,6).

calculations with total geometry optimization for altogether 32 one-periodic models of SW TiO₂ NTs of different chiralities and morphologies.

Four curves $E_{\text{strain}}(D_{\text{NT}})$ imaged in Fig. 7 for all four sets of titania nanotubes confirm conclusions drawn above from Tables 3–5. A ratio of the calculated strain energies between the

Table 5
The structural and electronic properties of four pairs of symmetry-compatible TiO₂ NTs^a.

Pairs of NTs with equal diameters	N_a	D_{NT} (Å)	l_{NT} (Å)	h_{NT} (Å)	d_{Ti-O} (Å)				q_{Ti} (e)	E_{relax} (eV/TiO ₂)	E_{strain} (eV/TiO ₂)	$\Delta\epsilon_{gap}$ (eV)
					Ti-O1	Ti-O2	Ti-O3	Ti-O4				
(2n) _n /m group, Figs. 5a and 6a												
3-layered (6,6)	36	10.06	2.99	1.86	1.89	1.94	2.00	2.05	2.42	-0.09	0.479	4.66 ⁽ⁱ⁾
6-layered (-3,3)	36	9.98	3.66	2.45	1.795	1.86	1.925	2.025	2.28	-0.82	0.175	4.92 ⁽ⁱ⁾
(2n) _n mc group, Figs. 5b and 6b												
3-layered (12,0)	72	11.70	5.10	1.88	1.915	1.945	1.96	2.03	2.43	-0.09	0.349	4.70 ⁽ⁱ⁾
6-layered (10,10)	120	11.85	10.39	2.46	1.80	1.835	1.945	2.02	2.27	-0.45	0.191	5.05 ^(d)
(2n) _n mc group, Figs. 5c and 6c												
3-layered (18,0)	108	17.23	5.12	1.90	1.935	1.95	1.965	1.965	2.44	-0.05	0.155	4.75 ⁽ⁱ⁾
6-layered (15,15)	180	17.33	10.33	2.43	1.785	1.87	1.92	2.01	2.27	-0.14	0.127	5.36 ⁽ⁱ⁾
(2n) _n /m group, Figs. 5d and 6d												
3-layered (12,12)	72	19.73	2.97	1.91	1.935	1.95	1.98	1.995	2.44	-0.04	0.117	4.77 ⁽ⁱ⁾
6-layered (-6,6)	72	19.84	3.54	2.39	1.765	1.87	1.92	2.11	2.19	-0.14	0.067	5.26 ⁽ⁱ⁾

^a Definition of values is the same as before Table 3 (Section 4.2).

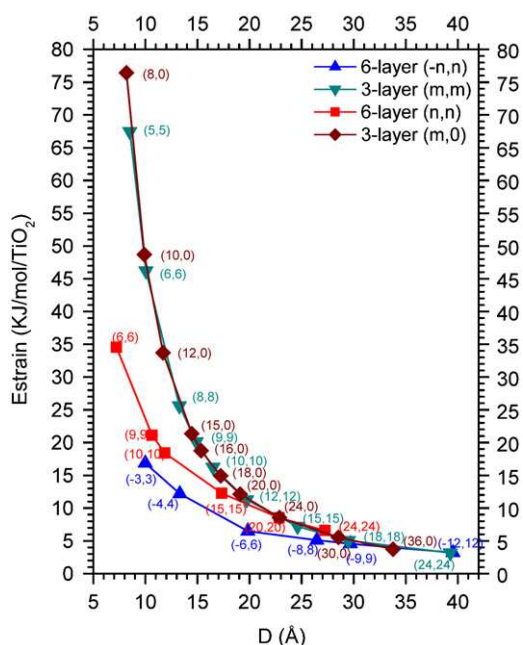


Fig. 7. The strain energy (E_{strain}) versus the nanotube diameter (D) for four sets of SW TiO₂ NTs: 3-layered structures with hexagonal (n,n) and ($n,0$) chiralities as well as 6-layered structures with centered rectangular ($-n,n$) and (n,n) chiralities.

3- and 6-layered titania NTs achieves 2–3 for nanotubes with diameters ≤ 10 Å and remains noticeable for those with diameters ≤ 20 Å, i.e., the 6-layered NTs are more stable energetically. When diameters of nanotubes increase up to 40 Å all the strain energies substantially decrease and approach each other. We wait that further increase in D_{NT} can result in slightly smaller values of E_{strain} for 3-layered nanotubes, since surface energy of the 3-layered titania slab has been found to be smaller than that of the 6-layered one (Table 2). Moreover, the strain energy of 6-layered NTs with ($-n,n$) chirality is smaller than that for (n,n) NTs of a similar diameter, which is in some contradiction with the results presented in Ref. [20]. This contradiction can be explained because the authors of that paper used the molecular mechanics for optimization of the nanotube structure while the first principles DFT method was applied by them for calculations on the electronic structure only. However, we use the hybrid PBE0

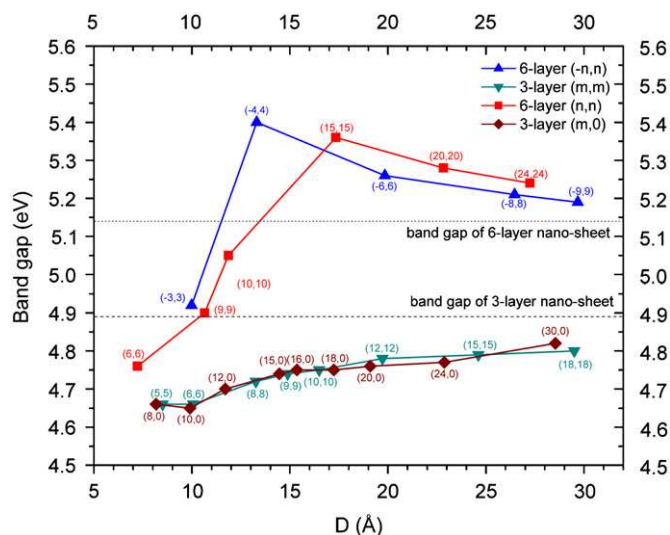


Fig. 8. The band gap ($\Delta\epsilon_{gap}$) versus the nanotube diameter (D) for four sets of SW TiO₂ NTs: 3-layered structures with hexagonal (n,n) and ($n,0$) chiralities as well as 6-layered structures with centered rectangular ($-n,n$) and (n,n) chiralities.

DFT-HF Hamiltonian both for the structure optimization and the electronic structure calculations. In the 3-layered nanotubes of similar diameters, the difference in strain energies for fluorite-type (n,n) and ($n,0$) chiralities is rather negligible, thus supporting qualitatively similar results obtained earlier for these types of nanotubes [17,18,21,25].

As was mentioned above, the lepidocrocite structures of titania sheets were earlier used for *ab initio* simulations on formation of TiO₂ nanotubes [26]. It should be noted that the authors of Ref. [26] used in their simulations the same computer code and the same PBE0 DFT functional as we have done in our study. We have compared the strain energy calculated by us for the 6-layered NTs derived from anatase with those obtained in Ref. [26]. This comparison shows that strain energy for TiO₂ nanotubes possessing a lepidocrocite-like structure is larger than that of same diameter NTs obtained from anatase layers. This may be the consequence of the presumably higher stability of the unrolled lepidocrocite-like TiO₂ layer compared to the corresponding anatase layer.

Fig. 8 presents four curves $\Delta\epsilon_{gap}(D_{NT})$. The band gaps of 6-layered titania nanotubes are found to be noticeably larger as

compared to those for the 3-layered NTs with the same diameter (Table 5). When these diameters markedly increase, their band gaps asymptotically approach those for the corresponding 2D slabs (Table 2). For the 6-layered titania nanotubes of both chiralities, the curves $\Delta\epsilon_{\text{gap}}(D_{\text{NT}})$ possess maxima at diameter range 13–17 Å, after which both the relaxation and strained energies of TiO₂ NTs substantially decrease. We again face discrepancy with Ref. [20] where the authors did not obtain such a relief for the curves $\Delta\epsilon_{\text{gap}}(D_{\text{NT}})$: their asymptotic reliefs are much closer to those obtained by us for 3-layered nanotubes (Fig. 8), which are qualitatively similar to band gap changes calculated earlier for hexagonal titania nanotubes [17,25].

Chemical nature of the Ti–O bonds in both 3- and 6-layered titania nanotubes is slightly different. Values of effective charges estimated by Mulliken population analysis on titaniums q_{Ti} presented in Table 5 clearly show that the chemical bonding in hexagonal nanotubes is more ionic. On the other hand, the calculated Ti–O bond populations in 6-layered NTs have been found to be 2–3 times larger than those in 3-layered slabs achieving 0.16–0.18 *e per* internal wall bonds, *i.e.*, the bonding in the former is a more covalent. We have calculated a series of the total and projected densities of states (DOS and PDOS) for TiO₂ anatase bulk (Fig. 4), 3, 6 and 12-layered titania sheets (Fig. 3) as well the selected 3- and 6-layered nanotube models shown in Figs. 5 and 6, respectively. Obviously, DOSs of 6- and 12-layered sheets as well as 6-layered nanotube are qualitatively similar to DOSs of bulk anatase. When increasing both D_{NT} and N_{a} , the profiles of DOSs and PDOSs become more complicated as the number of the one-electronic states increases. The total density of states projected on different atomic states imply that the states of the highest valence band (VB) mainly arise from the 2p states of oxygen atoms, while those of the lowest conduction band (CB) come from the 3d states of Ti atoms (Figs. 3–6). In 6-layered nanotubes, the contributions of O and Ti states in CB and VB states are found to be larger than in 3-layered nanotubes. It means that the O(2p)–Ti(3d) bond hybridization is more pronounced at PDOSs calculated for the equilibrium 6-layered TiO₂ nanotube structures, *i.e.*, their covalent bonding is stronger.

5. Conclusions

- In present study, we have applied the formalism of line groups for construction of titania nanotubes of different crystalline morphologies with rotohelical symmetry. The condition of the orthogonality of the nanotube chiral and translation vectors allows one to introduce a simple procedure for nanotube generation based on the rolling of a 2D supercell. The procedure suggested is applied to the 2D-periodic hexagonal, centered rectangular and primitive rectangular lattices formed from the bulk anatase.
- To analyze the structural and electronic properties of titania slabs and nanotubes, we have performed large-scale *ab initio* LCAO calculations using the hybrid Hartree-Fock/Kohn-Sham exchange-correlation functional PBE0 with the total geometry relaxation as implemented in the CRYSTAL-06 code [44]. To optimize the atomic basis sets, necessary for these calculations, we have applied the original program package OPTBAS interfaced with CRYSTAL-06.
- We have found that the structural optimization of the 3-layered slab results in a spontaneous (barrier-less) reconstruction to the hexagonal (1 1 1) fluorite structure. The structural optimization of 3- and 6-layered single-walled titania nanotubes, which symmetry can be described by either $(2n)_n/m$ or $(2n)_n/mc$ line groups, leads to growth of NT diameter for all morphologies considered.
- We observe noticeable differences between the calculated properties of 3- and 6-layered TiO₂ sheets and nanotubes. First of all, the strain energies of the 6-layered nanotubes are smaller than those of the 3-layered NTs of close diameters (for $D_{\text{NT}} \leq 20\text{--}25$ Å). The most probable reason of this 6-layered NT energetical stability is that in the 6-layered titania sheets and nanotubes with anatase structure both Ti sublayers are positioned in the middle between both the surfaces of sheets and nanotubes, *i.e.*, their formal bulk structure is O₂O–Ti₂–O₂O. On the other hand, the relaxation energies of the 6-layered NTs are larger than those for the 3-layered nanotubes (especially for small D_{NT}), due to a more complicated structure of the former. After several test calculations, we can predict that the SW nanotubes formed from the 12-layered (1 0 1) anatase slab are not stable.
- The band gaps of 6-layered titania nanotubes (typical semiconductor with $\Delta\epsilon_{\text{gap}} > 5$ eV) are found to be noticeably larger (up to 0.5 eV) as compared to 3-layered NTs with the same diameter. When these diameters markedly increase, their band gaps asymptotically approach those for 2D slabs of corresponding thickness. Chemical nature of the Ti–O bonds in both 3- and 6-layered titania nanotubes is slightly different: values of effective charges on titaniums clearly show that the bonding in hexagonal nanotubes is more ionic while higher Ti–O bond populations in 6-layered NTs (achieving 0.16–0.18 *e per* bond in internal wall) result in a more covalent bonding.

The present study can be considered as an initial step to gain a deeper theoretical insight into the technologically important TiO₂ nanomaterials. The next step is outlined to be a theoretical study on the double-walled titania nanotubes containing the two 3-layered NTs with different chirality indices.

Acknowledgments

R.E. is grateful to Prof. M. Damnjanović for stimulating discussions, S.P. is thankful for the financial support through the ESF project no. 2009/0216/1DP/1.1.1.2.0/09/APIA/VIAA/044.

References

- J. Zhao, X. Wang, T. Sun, L. Li, Nanotechnology 16 (2005) 2450.
- Y.Z. Li, N.H. Lee, E.G. Lee, J.S. Song, S.J. Kim, Chem. Phys. Lett. 389 (2004) 124.
- J. Choi, R.B. Wehrspohn, J. Lee, U. Gösele, Electrochim. Acta 49 (2004) 2645.
- R. Chu, J. Yan, S. Lian, Y. Wang, F. Yan, D. Chen, Solid State Commun. 130 (2004) 789.
- D.V. Bavykin, J.M. Friedrich, F.C. Walsh, Adv. Mater. 18 (2006) 2807.
- C.C. Tsai, H.S. Teng, Chem. Mater. 16 (2004) 4352.
- M.S. Sander, M.G. Cote, W. Gu, B.M. Kile, C.P. Trippie, Adv. Mater. 16 (2004) 2052.
- Y.H. Cho, G. Cho, J.S. Lee, Adv. Mater. 16 (2004) 1814.
- D. Li, Y.N. Xia, Nano Lett. 4 (2004) 933.
- R. Tenne, G. Seifert, Ann. Rev. Mater. Res. 39 (2009) 387.
- T. Maiyalagan, B. Viswanathan, U.V. Varadaraju, Bull. Mater. Sci. 29 (2006) 705.
- W. Wang, O.K. Varghese, M. Paulose, C.A. Grimes, J. Mater. Res. 19 (2004) 417.
- N. Viriya-empikul, N. Sano, T. Charinpanitkul, T. Kikuchi, W. Tanthapanichakoon, Nanotechnology 19 (2008) 035601.
- S. Zhang, L.M. Peng, Q. Chen, G.H. Du, G. Dawson, W.Z. Zhou, Phys. Rev. Lett. 91 (2003) 256103.
- R. Ma, Y. Bando, T. Sasaki, Chem. Phys. Lett. 380 (2003) 577.
- Q. Chen, G.H. Du, S. Zhang, L.M. Peng, Acta Cryst. B 58 (2002) 587.
- V.V. Ivanovskaya, A.N. Enyashin, A.L. Ivanovskii, Mendeleev Commun. 13 (2003) 5.
- A.N. Enyashin, G. Seifert, Phys. Status Solidi (b) 242 (2005) 1361.
- A.N. Enyashin, A.L. Ivanovskii, J. Mol. Struct.: THEOCHEM 766 (2006) 15.
- Z. Liu, Q. Zhang, L.C. Qin, Solid State Commun. 141 (2007) 168.
- J. Wang, L. Wang, L. Ma, J. Zhao, B. Wang, G. Wang, Physica E 41 (2009) 838.
- A.E. Vizitiu, M.V. Diudea, Studia Universitatis Babeş-Bolyai; Chemia (Romania), vol. 54, 2009, p. 173.
- F. Lin, G. Zhou, Z. Li, J. Li, J. Wu, W. Duan, Chem. Phys. Lett. 475 (2009) 82.
- A.V. Bandura, R.A. Evarestov, Surf. Sci. 603 (2009) L117.

- [25] T. He, M. Zhao, X. Zhang, H. Zhang, Z. Wang, Z. Xi, X. Liu, S. Yan, Y. Xia, L. Mei, *J. Phys. Chem. C* 113 (2009) 13610.
- [26] D. Szieberth, A.M. Ferrari, Y. Noel, M. Ferrabone, *Nanoscale* 2 (2010) 81.
- [27] M. Casarin, A. Vittadini, A. Selloni, *ACS Nano* 3 (2009) 317.
- [28] A.N. Enyashin, A.L. Ivanovskii, *J. Phys. Chem. C* 113 (2009) 20837.
- [29] Y. Noel, Ph. D'arco, R. Demichelis, C.M. Zicovich-Wilson, R. Dovesi, *J. Comput. Chem.* 31 (2010) 855.
- [30] Y.Q. Wang, C.G. Hu, X.F. Duan, H.L. Sun, Q.K. Hue, *Chem. Phys. Lett.* 365 (2002) 427.
- [31] F. Alvarez-Ramirez, Y. Ruiz-Morales, *Chem. Mater.* 19 (2007) 2947.
- [32] A. Vittadini, M. Casarin, *Theor. Chem. Acc.* 120 (2008) 551.
- [33] M. Damjanović, I. Milošević, *Line Groups in Physics: Theory and Applications to Nanotubes and Polymers. Lecture Notes in Physics*, vol. 801, Springer Verlag, Berlin, Heidelberg, 2010.
- [34] M. Damjanović, B. Nolić, B. Milošević, *Phys. Rev. B* 75 (2007) 033403.
- [35] H.T. Stokes, D.M. Hatch, B.J. Campbell, in: *ISOTROPY User's Manual*, Provo, UT, USA, 2007 <<http://stokes.byu.edu/isotropy.html>>.
- [36] V. Kopsky, D.B. Litvin (Eds.), *International Tables for Crystallography*, volume E, Subperiodic Groups, Kluwer Academic Publishers, Dodrecht/Boston/London, 2002.
- [37] C. Adamo, V. Barone, *J. Chem. Phys.* 110 (1999) 6158; M. Ernzerhof, G.E. Scuseria, *J. Chem. Phys.* 110 (1999) 5029.
- [38] M.M. Hurley, L.F. Pacios, P.A. Christiansen, R.B. Ross, W.C. Ermler, *J. Chem. Phys.* 84 (1986) 6840.
- [39] A. Schäfer, C. Huber, R. Ahlrichs, *J. Chem. Phys.* 100 (1994) 5829.
- [40] R.A. Evarestov, *Quantum Chemistry of Solids. The LCAO First Principles Treatment of Crystals. Springer Series in Solid State Sciences*, Vol. 153, Springer Verlag, Berlin, 2007.
- [41] B.D. Bunday, in: *Basic Optimization Methods*, Edward Arnold Ltd., London, 1984.
- [42] R.A. Evarestov, A.I. Panin, A.V. Bandura, M.V. Losev, *J. Phys.: Conf. Series* 117 (2008) 012015.
- [43] W.H. Press, S.A. Teukolski, V.T. Vetterling, B.P. Flannery, 3rd Ed., *Numerical Recipes in FORTRAN 77: The Art of Scientific Computing*, Vol. 1, Cambridge University Press, 2007.
- [44] R. Dovesi, V.R. Saunders, C. Roetti, R. Orlando, C.M. Zicovich-Wilson, F. Pascale, B. Civalleri, K. Doll, N.M. Harrison, I.J. Bush, Ph. D'Arco, M. Llunell, in: *CRYSTAL-2006 User Manual*, University of Turin, 2006 <<http://www.crystal.unito.it>>.
- [45] F. Labat, P. Baranek, C. Domain, C. Minot, C. Adamo, *J. Chem. Phys.* 126 (2007) 154703.
- [46] W.S. Su, T.C. Leung, C.T. Chan, *Phys. Rev. B* 76 (2007) 235413.
- [47] W. Hebenstreit, N. Ruzycski, G.S. Herman, Y. Gao, U. Diebold, *Phys. Rev. B* 62 (2000) R16334.
- [48] J. Muscat, V. Swamy, N.M. Harrison, *Phys. Rev. B* 65 (2002) 224112.